Supply-Limited, Climate-Driven Model for Holocene Spring Activity at Mickey Springs, Oregon, USA

L. Allen Mowbray and Michael L. Cummings

Portland State University

Keywords

Hot spring, climate, GPR, stratigraphy, elevation model

ABSTRACT

For hydrothermal systems with invariant conditions of heat source and permeable pathways, climate-driven changes in hydrologic conditions may dictate hydrothermal activity. Mickey Springs in the northwestern Basin and Range Province potentially reflects changing system dynamics in response to progressive drying of the Alvord valley from conditions of a pluvial lake to a high dessert. Ground penetrating radar (GPR) and elevation modeling are used here to interpret stratigraphic relationships in the context of this climate-driven model of spring dynamics. All springs appear to stratigraphically overlie, and are thus younger than, silicified delta sediments. Stratigraphic relationships have led to the hypothesis that pool size and degree of sediment infill of a spring can be roughly correlated to age, and that sinter deposition has been diminished with time. Currently, no sinter is being precipitated at Mickey Springs, and may indicate the exhaustion of groundwater supplied to the hydrothermal reservoir at the end of the Pleistocene by pluvial lake Alvord.

Introduction

The context of geothermal systems in active tectonic settings is potentially confounded by changing climate where the basic conditions of heat source and permeable pathways are met. The climate signal in geothermal systems includes hydrothermal explosion craters associated with draining of lakes during the deglaciation of the Yellowstone plateau (Muffler et al., 1971).

Mickey Springs in the northwestern Basin and Range Province potentially reflects changing system dynamics in response to progressive drying of the Alvord valley from conditions of a pluvial lake to a high dessert receiving less than 17 cm of precipitation a year (Western Regional Climate Center, 2014). Mickey Springs, one of three hot spring complexes in the Alvord Valley is within the Alvord Valley Known Geothermal Resources Area. However,

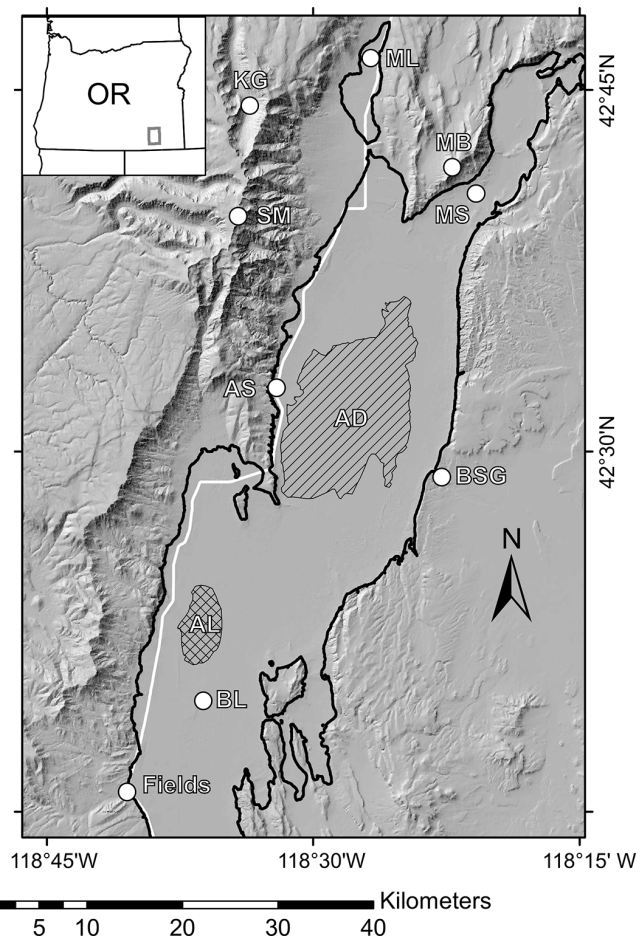

Figure 1. Location map of the Alvord Valley and Mickey Spring (MS) in southeastern Oregon. Highstand of Pluvial Lake Alvord is outlined in black at 1292 m, before outburst flood at Big Sand Gap (BSG) lowered lake level to 1280 m. Fields-Denio Rd represented by white line. Other hydrothermal features in the area: Borax Lake (BL) and Alvord Springs (AS) located at the foot of Steens Mountain (SM). Also located in image: Dry lakebed of Alvord Desert (AD, 1221 m), current extent of seasonally wet Alvord Lake (AL, 1227 m), community of Fields, Oregon, Kiger Gorge (KG), Mickey Butte (MB), Mann Lake (ML). Bath House Trench (Hemphill-Halley et al., 1989) located at Alvord Springs.

due to ecological conservation concerns, the Alvord Valley Known Geothermal Resources Area has not and will not be developed for geothermal energy. Additionally, Mickey Spring has been set aside as an Area of Critical Environmental Concern by the Bureau of Land Management (BLM) which manages the spring area.

Setting and Previous Work

The northwestern portion of the Basin and Range Province in Oregon is cut by faults with two principal orientations, NNE-striking and NW-striking. Scarberry et al. (2010) analyzed deformation of the NNE-striking Abert Rim fault and presented $^{40}Ar/^{39}Ar$ ages that allowed the temporal evolution of this fault system to be determined. They also used their interpretations of the Abert Rim fault as an analogue to the northwestern Basin and Range province to generalize a structural history of the greater area. The NW-striking faults in the northwestern Basin and Range Province formed prior to or coeval with development of NNE-striking faults. The deactivation of the NW-striking faults which are interpreted as dilational fractures (Scarberry et al., 2010) occurred as the tips of NNE-striking normal faults propagated northward. Through time, the extension on the NNE-striking faults has migrated from east to west (westward from Steens Mountain at ~10 Ma, Abert Rim after 8.7 Ma, to Cascade arc by ~5 Ma). Scarberry et al. (2010) interpreted the evolution of this system as response to the propagation of the Walker Lane transform and the San Andreas Fault Zone.

Mickey Springs lies in a northeast-trending arm of the Alvord Valley (Figure 1) and at the eastern edge of this propagating rift system (Hook, 1981). The valley is separated from the northern extension of the Alvord Valley and Steens Mountain by fault blocks including Mickey Butte. The topographically dominant Steens Mountain fault block lies on the west side of the Alvord Valley and the Alvord segment of the Steens fault zone lies at the base of the High Steens. The Alvord segment is a 27 km-long active fault and contains the youngest appearing fault scarps within the Steen fault zone (Hemphill-Haley et al., 1989). The Bath House trench near Alvord Hot Springs (Figure 1) was interpreted to demonstrate a total apparent vertical displacement of 3.3 m in a single event in the late Holocene (Hemphill-Haley et al., 1989). This young fault scarp cuts deposits from pluvial Lake Alvord (Oldow and Singleton, 2008).

Hook (1981) described the volcanic stratigraphy in the vicinity of Mickey Springs. The Steens Basalt was correlated to flows exposed to the east of the springs as well as to the west on Mickey Butte. The Steens Basalt was overlain by the "Mickey ignimbrite" in both settings and, in turn, the ignimbrite was overlain by the "Mickey basalt". The ignimbrite contains a 4.5 m thick vitric welded zone with poorly welded zones above and below. Cummings (1995) reported $^{87}Sr/^{86}Sr$ ratio for the ignimbrite of 0.716642 (±0.000032). The "Mickey basalt" is a series of dark, aphanitic and aphyric flows with total thickness of 120 m (Hook, 1982).

Oldow and Singleton (2008) used terrestrial laser scanning to analyze the Quaternary displacement on faults bounding the Pueblo basin (southern Alvord Basin, Figure 1) and within the basin. The resolution of this survey is 5 cm based on real time kinematic (RTK) GPS and terrestrial laser scanning (TLS). They used TLS scans and previous authors' shoreline dates for pluvial Lake Alvord to estimate the timing of displacements on faults offsetting those shorelines. Two sets of Pleistocene wave-cut terraces for pluvial Lake Alvord were recognized in the Pueblo basin (Oldow and Singleton, 2008). The older set, the Serrano terrace series (three terraces), has a high stand terrace (1308 m) estimated as forming between 200-130 ka. The younger terrace series, the Alvord terrace series (five terraces), had a high stand terrace (1287 m) estimated as forming between 20-15 ka.

The overtopping of the Thule Rim escarpment at Big Sand Gap in the Alvord basin and partial draining of pluvial Lake Alvord are documented by Carter et al. (2006), with stabilization of the shoreline at 1280 m. The precision of the terrestrial laser scanning survey by Oldow and Singleton (2008) indicates this shoreline is at 1277 m.

Oldow and Singleton (2008) also estimated that nearly 50% of the total offset of lake shorelines occurred on the western margin of the basin; nearly 30% of the displacement was on structures within the basin and 20% was accommodated by faults in the highlands east of the basin. The extent and complexity of displacement on faults associated with the basin was found to be greater than previously determined (e.g. Carter et al., 2006).

The elevations of paleoshorelines for pluvial Lake Alvord by Carter et al. (2006) were determined by GPS location and corresponding elevation from 1:24000 scale contour maps, and described at 1310, 1305, 1292, 1287, and 1280 m. The most prominent are at 1292 and 1280 m. In Mickey basin, a small topographically closed basin north of Mickey Springs, the 1292 m shoreline features include laterally continuous barrier beaches (Carter et al., 2006). The most prominent shoreline features are at ~1280 m; the elevation of the outflow channel at Big Sand Gap (Figure 1) (1277 m elevation of Oldow and Singleton, 2008). The shoreline in Figure 1 is based on the 1292 m elevation of Carter et al. (2006) because, though it is less precisely measured, the work was conducted in the Alvord and Mickey basins, and offsets of faulted shorelines make correlation of elevations in the Pueblo basin from Oldow and Singleton (2008) north into Mickey basin problematic.

Although ages of shorelines in the Alvord Valley are routinely correlated to those of pluvial Lake Lahontan in Nevada, Carter et al. (2006) reported two age determinations from Mickey Basin and at the base of Mickey Butte west of Mickey Springs. Tephra collected at 1243 m at the base of Mickey Butte was correlated to the Mt. St. Helens set Sg ash (a summary of pre-1980 ash deposits from Mt. St. Helens can be found in Mullineaux, 1986). The characteristics of these lacustrine silts suggest low-energy, deep-water environment at the time of tephra deposition which Clague et al. (2003) estimated to have an age of 13,350 – 14,400 ^{14}C yr B.P. Carter et al. (2006) argued that open-basin conditions produced by overflowing of pluvial Lake Alvord at Big Sand Gap into the Crooked Creek drainage to the east existed near the time of the deposition of the Mt. St. Helens tephra at ~ 14-13 ^{14}C ka.

The hot springs at Mickey Springs were studied by Cummings and St. John (1993a) in conjunction with studies at two other hot springs in the Alvord/Pueblo valleys (Borax Lake and Alvord Hot Springs). Figure 2 illustrates two main features of the site: silicified lithic-rich delta sands (outlined in blue) and the area of sinter

deposits and active springs. The delta sands crop out immediately west of the active hot spring area and include well-developed top-set, fore-set, and bottom-set beds. The fore-set beds are up to 1.8 m thick. Current ripple marks are present in moderately silicified, medium-grained sandstone. Scour and fill cross sets contain masses of partially permineralized wood chips and stem fragments. The wood was too permineralized for carbon-14 dating (1992 technologies). The elevation of the highest part of the delta deposit is 1247 m.

Locally within the delta, lithic grains float in silica sinter indicating co-deposition of sand and silica sinter. Point counts of thin sections cut from these layers indicate 28 to 45 percent of the samples are brown spotted, uniform brown, and clear, colorless silica (Cummings and St. John, 1993a). U-Th disequilibrium series dating was conducted at Argonne National Laboratory. The determination indicated the silica was deposited less than 16,000 years before present.

Silica sinter overlies fine-grained, silica-cemented sandstone near the eastern edge of the delta deposit, but over a variety of substrates as one moves farther from the delta outcrops (delta outlined in blue, Figure 2). X-ray diffraction analysis indicates the sinter is opal-A, amorphous silica, with trace amounts of quartz and feldspar (Cummings and St. John, 1993a). The quartz and feldspar are interpreted as aeolian sediment deposited during sinter precipitation. Oestreicher (2004) examined the morphology and microbial communities preserved in this sinter for five samples collected from three vents, one active but not precipitating silica sinter and two fossil vents (Figure 2). Cast and mold structures were common and based on SEM analysis of these samples compared to living organisms examined in the outflow channel from the highest temperature springs (Figure 2) the fluid temperatures at the edges of extinct hot springs pools was between 60° C and 40° C.

Reservoir conditions for the Mickey Springs system were estimated by Cummings and St. John (1993a) using a variety of methods. The following is summarized from their findings unless otherwise noted. Gas chemistry (14-June-1992) was 99.3 volume % water (0.612 volume % CO_2). The gas sample was collected from the highest temperature vent (94.6°C). Reservoir temperatures were estimated for a variety of chemical geothemometers applied to water sample data collected approximately every 3 months over 15 months. The highest temperatures were obtained for the conductive quartz, Na-K-Ca, and K/Na geothermometers between 190° and 199°C. The $^{18}O_{(SO4\text{-}H2O)}$ geothermometer yielded temperature of 150° C. The average mean residence time of the water discharging from Mickey Springs was estimated from tritium analysis. The samples were collected 3-September-1992 and contained 0.10 tritium units (error ± 0.09 T.U.). Using a piston flow model residence time was 73 years while using a well-mixed model the age was 8,525 years (Shevenell, 1990).

Current Study

In 2014, we began a study of the Mickey Springs system to test two models for controls on spring activity: 1) transport limited, structurally controlled model and 2) supply-limited, climate driven model. Both models assume a constant source of heat related to ongoing Basin-and Range extension as proposed by Cummings and St. John (1993a), and do not require establishment of an exact onset time for hydrothermal activity, but describe the pattern of spring activity after initiation and delta silicification. In this paper, we set out the two models and explore the supply-limited, climate driven model.

The first model is transport-limited and structurally controlled, assuming that a continuous supply of hydrothermal fluid exists at depth. Many hydrothermal systems, including Mickey Springs (Anderson and Fairley, 2008), are attributed to increased permeability at a stepover dilation zone between two interacting fault tips (Sibson, 1987). Spring migration has been attributed to cementation of permeable pathways from silica deposition diminishing spring activity over time and the development of new springs as new permeable pathways open through fault propagation at dilation zones (Curewitz and Karson, 1997). Historical observations have correlated seismic activity with increased spring discharge at Mickey Springs (personal communication with Rick Wells, BLM staff Geologist, Burns District, February 2014) and in general through the Alvord Valley (Hemphil-Haley et al., 1989).

The second model is supply-limited and climate driven and attributes the apparent discrepancy between current spring activity and extent of past sinter deposition to a lagged hydraulic response to

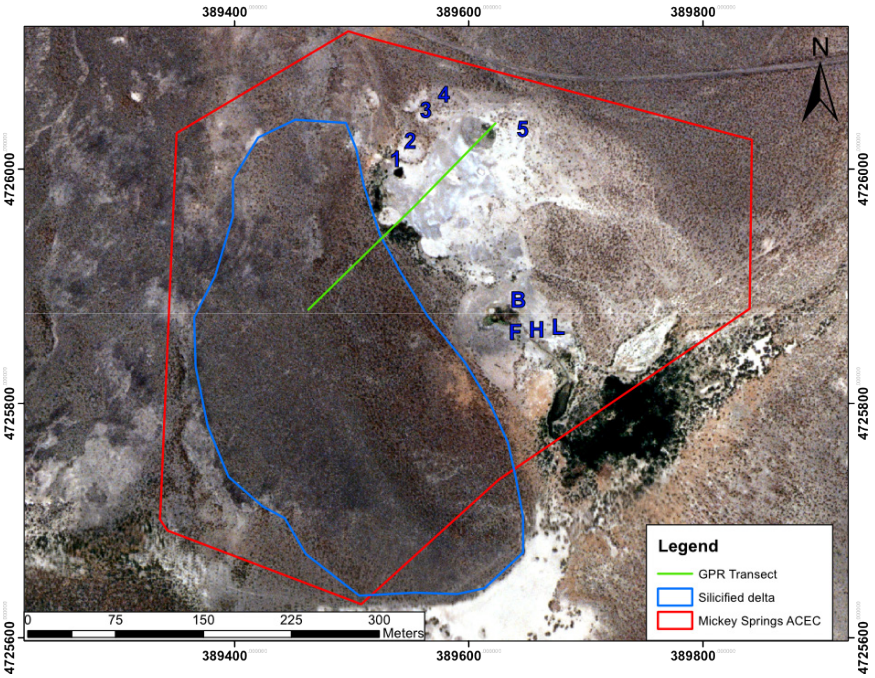

Figure 2. Aerial photograph of Mickey Springs showing the distribution of two main features: the rocks of a silicified delta consisting of conglomerates and sandstone (blue outline), and silica sinter deposits (white) surrounding hot spring vents. The red box shows the boundaries of the Mickey Springs Area of Critical Environmental Concern. The green line shows the trace of a ground-penetrating radar (GPR) transect across the area of silica sinter deposits and the silicified sandstone of the delta. Locations shown in blue of sinter (1-5) and microbial (B, F, H, L) samples used by Oestreicher (2004).

the drying and warming of the climate at the end of the Pleistocene. We propose that when pluvial Lake Alvord was present it provided water to deeply circulating flow paths and may have initiated spring activity at the end of the Pleistocene. Currently, earthquake rupture may maintain permeable pathways, but the hydrothermal fluid available to the system has been diminished with the drying of the lake and groundwater supply. Few studies have examined the role of changing climate on the dynamics of geothermal systems. Muffler et al. (1971) and Browne and Lawless (2001) examined these relations in Yellowstone National Park and New Zealand, respectively.

Methods

A field survey of spring mounds identified recognizable spring features and quantified spring surface dimensions (Table 1). Follow-up studies using photogrammetry, ground penetrating radar (GPR), soil probes, and thermoluminescence dating are being used to investigate surface morphology, subsurface characterics of active and inactive vents, and age constraints on vent activity and sinter deposition.

Elevation data at Mickey Springs were obtained through a photogrammetric process known as Structure from Motion (SfM) where a series of photos of the spring area taken from multiple elevated positions (in this case, a camera on an extended pole) are digitally processed using Microsoft Photosynth to create an elevation point-cloud. This point cloud was georeferenced in Cloud Compare through a matrix transform based on GPS coordinates and surveyed elevations of photographed objects. Elevation control was based on NAVD 88 orthorectified elevation of National Geodetic Survey benchmark 28 STR of 1247.101 m. The georeferenced pointcloud was then used to create a digital elevation model (DEM) usable in GIS programs. The model is used here to compare elevations and dimensions of spring features.

Ground penetrating radar (GPR) is a nondestructive field technique that uses radar pulses to image the shallow subsurface. A GPR transect was conducted on-site in December 2013 using 250 MHz antennae to identify GPR signatures of specific stratigraphic layers (sinter, host material, pool fill) to 2 m below the surface. This subsurface model was topographically corrected from slope breaks surveyed with a total station and georeferenced using GPS.

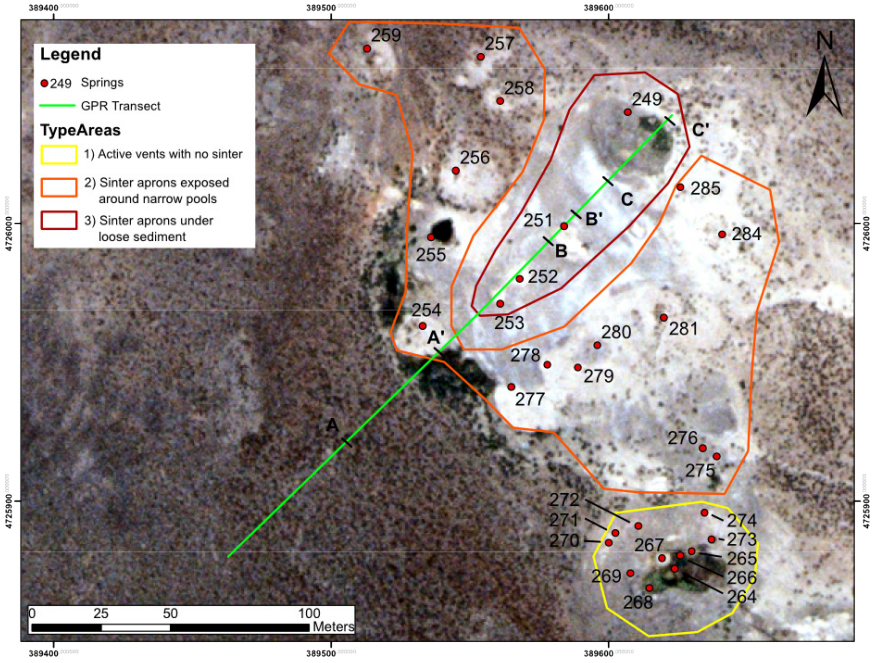

Figure 3. Identified spring features described in Table 1. Springs are classified into three groups based on morphologic relationships: 1) active vents without associated sinter, 2) active and inactive vents associated with silica sinter mounds, 3) active and inactive vents associated with sinter mounds buried beneath fine-grained sediment. Three GPR sections A to A′, B to B′, and C to C′ are shown in Figures 6, 7, and 8, respectively.

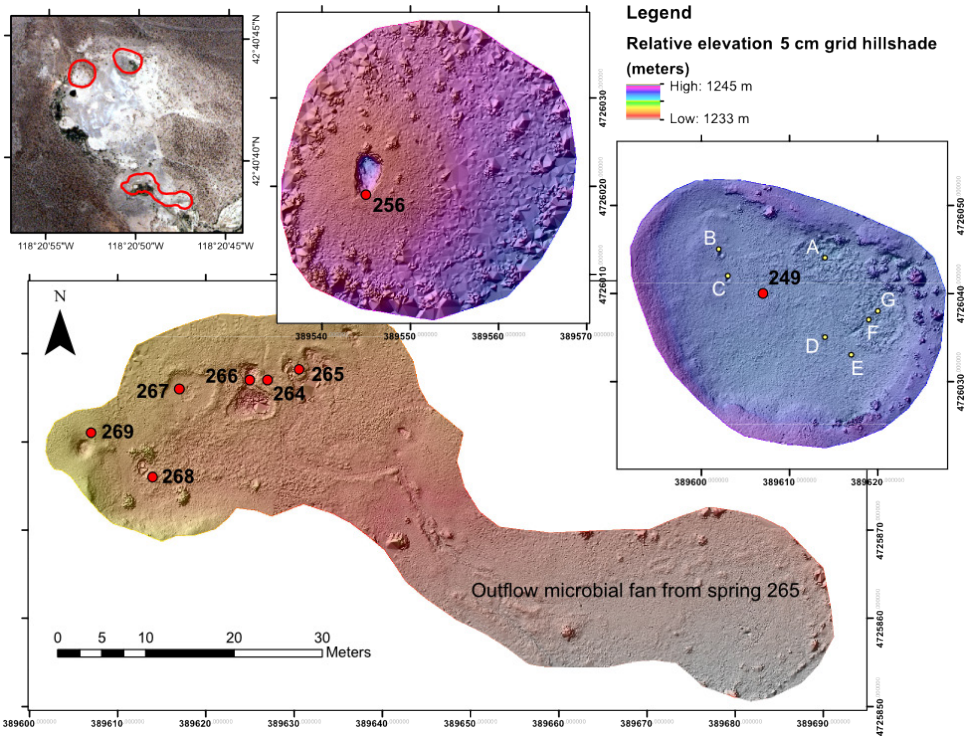

Figure 4. 5 cm resolution elevation models of three springs, colored by elevation as indicated in the legend, and overlaid with a 30% transparent hillshade to show texture. The three models represent the three types of spring morphologies at Mickey Springs. Springs 264-266 and mud pots 267-269 have no evident sinter, but are the major sources of thermal flux at Mickey Springs (group 1). Spring 256 has an extensive sinter apron around a narrow, unfilled inactive vent (group 2). Spring 249 is a broad, sediment-filled, sinter-rimmed pool (group 3). Temperatures of remnant activity in spring 249 (A-G) are listed in Table 1.

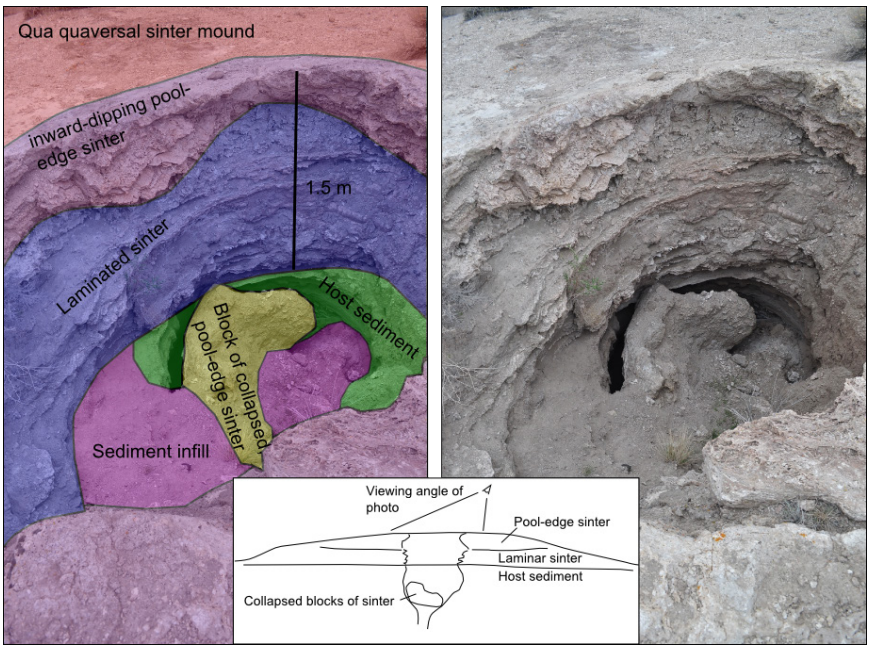

Figure 5. Photograph and stratigraphy of spring 256. Inward dipping pool-edge sinter (purple) and laminated sinter (blue) forms the top one and one-half meters of the pool mound, covering host sediment (green) exposed in the dry spring pool. Blocks of pool-edge sinter (yellow) have broken from the rim and infill the pool, an some sediment infill (pink) is also present.

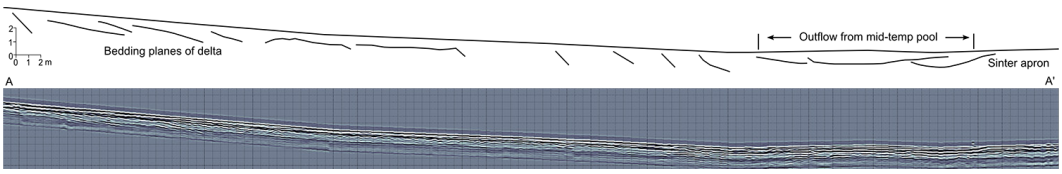

Figure 6. GPR section A to A′, crossing from the slope of the silicified delta, across the vegetated outflow channel of spring 255 to the edge of the sinter apron of spring 254. Bedding planes of the delta are visible in the GPR data, as well as infill features of the outflow channel, possibly indicating channel migration over time. Refer to Figure 3 for locations of spring 254 & 255.

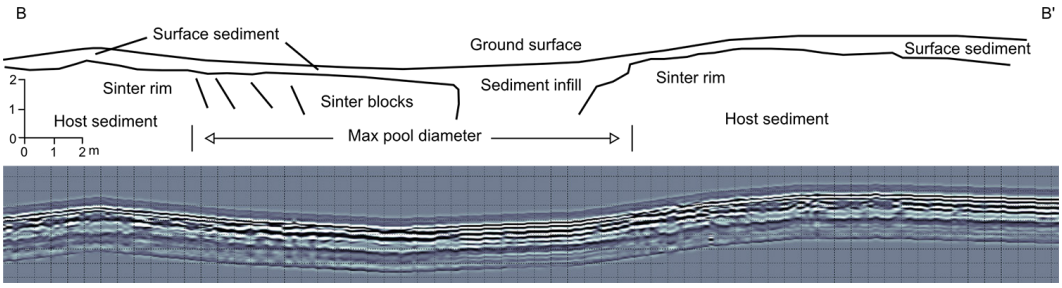

Figure 7. GPR section B to B′, across inactive spring 251. Sinter is not visible in the low relief, sediment-covered pool rim, but blocks of sinter are visible at the center of the pool floor. An area of thinly bedded sediment, free of sinter blocks, is visible in the GPR data. Refer to Figure 3 for location of spring 251.

Spring Mound Survey and Elevation Models

During the spring mound survey, three general field relations were identified and are summarized in Figures 3 and 4. Figure 3 shows the spatial distribution of 1) active vents without associated sinter, 2) active and inactive vents associated with silica sinter mounds, and 3) active and inactive vents associated with silica sinter mounds, but buried beneath fine-grained, low density sediment. Figure 4 provides photogrammetric elevation models for each type of field relation. Specific spring dimensions and temperatures of active gas vents, mudpots, and springs are listed in Table 1.

1. Active vents without associated sinter are located to the south and at the lowest elevation (1232 m) and are irregular in shape. These vents include mudpots (69 to 95°C), hot springs (28 to 91° C), and hot ground (44 to 95° C) in a 50 x 50 m area and 5 m below most other springs. Although calcite deposits are present along the outflow channel from the highest temperature springs, silica sinter is not present. This area contains the majority of high temperature springs, one of which was observed to geyser in 1993 (Cummings and St. John, 1993b). The highest ground temperatures were measured here indicating an area of high heat flux.

2. The second spring morphology is mostly inactive springs with extensive qua quaversal sinter aprons exposed surrounding a narrow (average diameter of 4.7 m) pool with inward dipping pool-edge sinter (points 254-259, and 275-285, Figure 3). Springs 254-259 lie to the north of the sediment-covered springs (described below), and increase slightly in elevation to the north (up to 1240 m). Springs 275-285 lie south of the sediment covered springs, and typically have mounds elongated along the south dipping slope from the higher elevation, sediment covered springs (1236 m) to the lower elevation, high temperature area (1231 m). Spring 256 has typical morphology, but has much less sediment infill than other springs of this type. The elevation model for spring 256 is shown (Figure 4) to relate the broad sinter apron relative to the narrow pool opening. Elevation modeling of this spring was selected for its exposure of vent stratigraphy, made available by the lack of sediment infill. In the inactive vent, 0.5 m of inward-dipping pool-edge sinter overlies 1 m of laminated sinter, which overlies unconsolidated lithic-rich sandy host sediment (Figure 5). A large block of sinter, broken from the pool rim, is present in the bottom of the pool.

3. The third type of spring morphology includes one active and three inactive springs with average diameter of 21 m, extensively covered by loose, fine grained white sediment (points 249-253, Figure 3). This sediment reacts with HCl, which indicates a high carbonate content. Spring morphology consists of an open pool from 11-31 m in diameter, surrounded by a qua quaversal mound. A typical pool is infilled with fine grained sediments, and blocks of sinter are present in the pool infill and some pool-rim sinter is exposed. Sediments infilling pools and covering mounds were probed with a metal rod, which met refusal generally within 10 cm of the surface, indicating a sinter apron surrounding the pools and blocks of sinter infilling the pools. Spring 249 is

Table 1. Spring mounds identified in 3/14 field survey.

Site #	Description	Temp (°C)[1]	Pool crest diameter (m)[2]	Max pool/rim relief (m)[3]	Max mound relief (m)[3]	Easting[4]	Northing[4]	Grouping in Figure 3
249	Largest pool diameter in spring complex. Sediment infilling pool, with blocks of sinter exposed in rim and collapsed in blocks in pool floor. Areas of remnant spring activity (A-G) in pool, but largely inactive. All temperatures from small pools with no outflow except gas vent at point C.		32.05	1.77	2.83	389607	4726040	3
A		57				389614	4726044	
B		73				389602	4726045	
C		31				389603	4726042	
D		61				389614	4726035	
E		63				389617	4726033	
F		52				389619	4726037	
G		48				389620	4726038	
251	Inactive, sediment filled pool. No sinter visible at lip, but small mound of sinter at center of infilled pool protruding from sediment.		21.25	0.934	0.752	389584	4725999	3
252	Two overlapping pools, both inactive and infilled with sediment. No sinter visible around rim, covered with white sediment.		19.55	1.125	1.125	389568	4725980	3
253			11.65	0.575	0.56	389561	4725971	3
254	Inactive sediment filled pool. Outflow from 255 flows around this sinter mound.		3.2	0.243	1.251	389533	4725963	2
255	Low temperature pool of upper tier springs.	48	10.05	0.468	0.468	389536	4725995	2
256	Inactive spring with sinter armor around vent. See Figure 5.		3.3	2.61	2.61	389545	4726019	2
257	Inactive, sediment filled spring, extensive sinter armor around small vent completely filled with sediment and blocks of broken sinter.		3.55	0.335	0.468	389554	4726060	2
258	Inactive, sediment filled spring, extensive sinter armor around small vent completely filled with sediment and blocks of broken sinter.		3.35	0.119	1.008	389561	4726044	2
259	Sinter apron evident, with narrow, sediment filled vent.		4.9	0.103	1.127	389513	4726063	2
264	Bubbling pool of warm water, extensive films of floating microbial mats at or near surface of water.	28	4.9	0.2		389625	4725887	1
265	Hot source of spring water, major source of spring outflow volume in spring complex.	88	5.7	0.2		389628	4725888	1
266	Bubbling mud pot between springs.	86	0.2	0.2		389627	4725887	1
267	Expansive area of dry hot ground, with low-relief individual mud pots bubbling in center.	92	6.5	0.1		389617	4725886	1
268	Roiling mud pit, bubbling with gas, cloudy light brown water.	69	1.8	0.25		389614	4725876	1
269	Mud pot bubbling with multiple vents. High surrounding rim.	95	3.5	1.12		389607	4725881	1
270	Dry hot ground in slight depression.	95				389601	4725885	1
271	Dry hot ground in slight depression.	67				389600	4725892	1
272	Dry hot ground in slight depression.	83				389605	4725894	1
273	Hot spring vent, no outflow, 3 separate vents with water present below ground surface.	91	3.6	0.14		389638	4725894	1
274	Dry hot ground.	44				389641	4725901	1
275	Small active spring pool, no current outflow but visible established outflow channel into inactive spring 276.	48				389639	4725916	2
276	Sediment infilled pool, no outflow and water in pool is well below exterior ground surface. Spring remnant activity is located on periphery of spring pool sediment floor along vertical fracture in sinter.	75	3.6	1.297	0.724	389634	4725919	2
277	inactive spring on incline between upper and lower spring bench, filled with sediment to near sinter rim.		3.4	0.294	2.51	389565	4725941	2
278	Fracture between springs forming pools of water.	39	0.85	0.25		389578	4725949	2
279	small vent with sinter armor 36 cm thick above exposed host sediment, water 30 cm below sediment, sinter transition.	45	0.2	0.36		389589	4725948	2
280	inactive spring, sinter exposed on rim of infilled pool.		16.45	2.485	2.268	389596	4725956	2
281	Sinter rim overhang, sediment filled pool with 1/4 of pool bottom occupied by cloudy brown water and green microbe mats.	45	4.95	0.997	2.229	389620	4725966	2
284	Extensive sinter roof completely covering spring, no visual evidence of outflow, but thickness of sinter (0.4m) is exposed by collapsed block, which reveals cavern extending for 2.8 m laterally and 0.6m vertically down to sediment infill.		-1.5	0.31	2.413	389641	4725996	2
285	Circular, inactive sinter mound, sediment filled, sinter rim broken in blocks.		3	0.185	0.456	389626	4726013	2

[1] Temperatures recorded with Vernier temperature probe (+/- 0.5°C).
[2] Pool dimensions measured by tape measure (+/- 1 cm) on east-west and north-south axis
[3] Elevations measured with Sokkia Set 4BII total station (+/- 1 cm).
[4] Positions recorded by Garmin GPSmap 60CSx GPS (+/- 2 m)

representative of these features, and an elevation model of spring 249 is shown in Figure 4, in addition to a GPR transect in Figure 8, which shows the sinter apron around the pool rim, as discussed in the next section of this paper. Remnant spring activity persists in the form of a gas vent (31° C) and small spring pools (up to 50 cm diameter, 48-73°C) that have no outflow.

Ground Penetrating Radar

The GPR antennae used here were able to image approximately 2 m of the subsurface. A 200 m transect of GPR data was collected, as indicated by the line in Figure 3. The 2 m deep cross section was successful in distinguishing sinter, host material, and pool infill. Three subsections of the GPR transect are described below.

Bedding planes of the silicified delta are apparent in section A to A' (Figure 6). These bedding planes are interpreted to extend under the vegetated outflow from spring 255 and the sinter apron of spring 254. Also visible in the GPR profile is evidence of migration of the outflow channel. The sediments of the outflow overlie the apron of spring 254, indicating that 254 became inactive, then outflow of 255 initiated and flowed around the pre-existing mound, where vegetation began to colonize and trap sediment, depositing above the sinter apron.

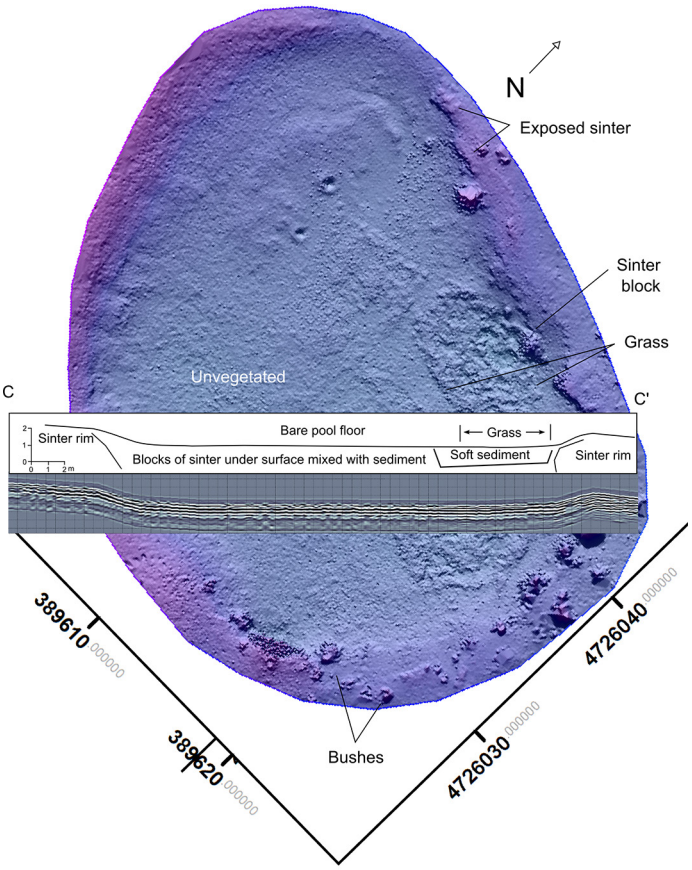

Figure 8. GPR section C to C′ superimposed over its location on the elevation model of spring 249. Sinter is exposed on the edges of the pool. The floor of the pool is filled with sediment to a minimum of 1.7 meters below the pool rim. GPR profile reveals many blocks of sinter ensconced by infilling sediments. Refer to Figure 3 for location of spring 249.

Sediments and blocks of sinter infilling spring pools are also visible in the GPR profile. Section B to B' (Figure 7) shows pool edge sinter overlying host sediment around the pool-edge of spring 251. No sinter is visible on the surface, but is overlain by 10 cm of the carbonate-bearing soils described above. Sinter is observed in the center of the pool. This is interpreted as blocks of pool-edge sinter, collapsed into the pool as the pool was filling with sediment. The 2 m deep, thin horizontal bedding of sediment infill free of sinter blocks was confirmed by probing with a metal rod which easily penetrated the sediment, unlike other areas where refusal was encountered just below the surface.

GPR segment C to C' is shown superimposed over its location on the elevation model of spring 249 (Figure 8). Thick horizontal bedding is evident in the northeast third of the pool infill, where grass is present. Sinter is exposed in much of the pool rim, as well as broken blocks of sinter lying on the northeast pool floor. Remnant spring activity is found in vents across the sediment infill, and provides water for the vegetation in the pool infill (rough texture in elevation model).

Discussion

The supply-limited, climate-driven model explores relations between the late Pleistocene and Holocene histories of Mickey Springs. In a general sense, the availability of water decreases through this time from the pluvial lake conditions of the late Pleistocene to the modern high desert conditions. If this model correctly describes these changing conditions, then the modern system will continue to adjust to ongoing drying of the basin.

Timing and Water Availability

The sedimentology of the silicified conglomerates and sandstones suggests sediment accumulation as water depth decreased. The upward progression from thinly bedded, fine-grained sandstone, to conglomeratic bottom-, fore- and top-sets, to scour and fill cross bedding and ripple marks in interbedded conglomerate and coarse-grained sandstone is the basis of this interpretation. The elevation of the uppermost deposits, 1247 m, is well below the prominent strand line associated with the overtopping of the Big Sand Gap barrier at 1280 m (Carter et al., 2006).

Coeval deposition of silica sinter with sand and gravel indicates system capability of producing colloidal silica during this phase of deposition. Although U-Th disequilibrium dating failed to yield a date, the indication of deposition of sinter after 16,000 years before present sets an upper limit on these conditions. The timing can be further constrained by dates produced by Carter et al. (2006) and Oldow and Singleton (2008). Oldow and Singleton (2008) suggest a low stand of pluvial Lake Alvord at about 1238 m to 1246 m based on archaeological work of Pettigrew (1984). Arrow heads in this elevation range were estimated between 10 and 12 ka.

Conceptual Model

As lake depth decreased below the current upper elevation of the silicified delta, condition of spring activity necessarily changed from sub-aqueous to sub-aerial. The sediment-covered spring with

larger pools are interpreted to be the oldest springs, as evidenced by the broken state of the pool-edge sinter and degree of sediment infill in the inactive pools. These infilling, fine-grained sediments are interpreted as the continued supply of quartz and feldspar grains of wind-blown sediment (as described by Cummings and St. John, 1993a), but now settling into an inactive spring pool instead of incorporated into sinter.

The broad-shielded mounds with narrow pools and extensive pool-edge sinter are interpreted as younger than the larger, sediment-covered pools, but are older than the current high-temperature area of mudpots and hot springs at lower elevation. This is evidenced by the varying states of sediment infill. The narrower pool vents are interpreted as indicating a diminished outflow (not capable of eroding a large pool) and cooling spring temperatures, allowing increased precipitation of sinter at the pool rim.

Substrate for the main sinter deposits varies. Near the outcrops of silicified sandstone and conglomerate the substrate for sinter is thin-bedded, fine-grained sandstone. These relations are consistent with GPR data in Figure 6. Elsewhere, sinter deposits directly overlie unsilicified fossil soils with root seats lined with opaline silica (Cummings and St. John, 1993a) illustrated in Figure 5.

Sinter deposition ceased at some point as the recharge once provided from pluvial lake Alvord has been exhausted. The sinter deposits are primarily located at elevations between 1240 m and 1234 m. Remnant spring activity persists on this upper platform in the form of seeps and springs with temperatures that range from 31°C to 73°C (Table 1), but the majority of outflow is from a single spring at 48 °C (Spring 255).

The modern, higher temperature springs and mudpots are present at lower elevations between 1230 m and 1232 m. The temperature of springs at this lower elevation span between 28°C and 95°C. The majority of spring outflow comes from a single source that has shown persistent, near-boiling temperatures for at least 20 years, but has no sinter deposition. The lack of sinter at this lower elevation could indicate that the entirety of activity has been recent, after conditions of sinter precipitation had ceased.

Conclusions

The supply-limited, climate-driven model is supported by the lack of current sinter precipitation in comparison to older evidence of hydrothermal activity. All springs appear to stratigraphically overlie, and are thus younger than, silicified delta sediments. Stratigraphic relationships have led to the hypothesis that pool size and degree of sediment infill of a spring can be roughly correlated to age, and that sinter deposition has diminished with time. Currently, no sinter is being precipitated at Mickey Springs, and may indicate the exhaustion of groundwater supplied to the hydrothermal reservoir at the end of the Pleistocene by pluvial Lake Alvord.

References Cited

Anderson, T. R., and J. P. Fairley, 2008, Relating permeability to the structural setting of a fault-controlled hydrothermal system in southeast Oregon, USA: Journal of Geophysical Research: Solid Earth, v.113, B05402.

Browne, P. R. L., and J. V. Lawless, 2001, Characteristics of hydrothermal eruptions, with examples from New Zealand and elsewhere: Earth-Science Reviews, v.52, p. 299-331.

Carter, D. T., L. L. Ely, J. E. O'Connor, and C. R. Fenton, 2006, Late Pleistocene outburst flooding from pluvial Lake Alvord into the Owyhee River, Oregon: Geomorphology, v. 75, p. 346-367.

Clague, J. J., R. Barendregt, R. J. Enkin, and F. F. Foit, 2003, Paleomagnetic and tephra evidence for tens of Missoula floods in southern Washington: Geology, v. 31, p. 247-250.

Cummings, M. L. and A. M. St. John, 1993a, Hydrogeochemical characterization of the Alvord Valley Know Geothermal Resources Area Harney County, Oregon: final report to the Bonneville Power Administration under Agreement No. DE-PR79-91BP19408.

Cummings, M. L. and A. M. St. John, 1993b, Hot-spring sinter deposits in the Alvord-Pueblo Valley, Harney Couny, Oregon: Geological Society of America, Abstracts with Programs, v. 25,

Cummings, M. L., 1995, Extent and location of the geothermal aquifer in the Alvord basin, Harney County, Oregon: A study based on strontium isotope geochemistry of rocks and fluids: final report to the Bureau of Land Management under Purchase Order No. 1422H952-P4-4885.

Curewitz, D. and J. A. Karson, 1997, Structural settings of hydrothermal outflow: Fracture permeability maintained by fault propagation and interaction: Journal of Volcanology and Geothermal Research, v.79, p. 149-168.

Hemphill-Halley, M. A., W. D. Page, R. Burke, and G. A. Carver, 1989, Holocene activity of the Alvord fault, Steens Mountain, southeastern Oregon: final report to the U.S. Geological Survey under Grant No. 14-08-001-61333, 45 pp.

Hook, R. C., 1981, The volcanic stratigraphy of the Mickey Hot Springs area, Harney county, Oregon [M.S. thesis]: Corvallis, Oregon, Oregon State University, 66 p.

Muffler, L. J. P., D. E. White, and A. H. Truesdell, 1971, Hydrothermal explosion craters in Yellowstone National Park: Geological Society of America Bulletin, v. 82, p. 723-740.

Mullineaux, D. R., 1986, Summary of pre01980 tephra-fall deposits erupted from Mount St. Helens, Washington State, USA: Bulletin of Volcanology, v. 48, p. 17-26.

Oestreicher, Z. W. J., 2004, Geomircrobiology investigation of Mickey Hot Springs, southeastern Oregon [M.S. thesis]: Portland, Oregon, Portland State University, 171 pp.

Oldow, J. S. and E. S. Singleton, 2008, Application of Terrestrial Laser Scanning in determining the pattern of late Pleistocene and Holocene fault displacement from the offset of pluvial lake shorelines in the Alvord extensional basin, northern Great Basin, USA, Geosphere v. 4.3: p. 536-563.

Scarberry, K. C., A. J. Meigs and A. L. Grunder, 2010, Faulting in a propagating continental rift: Insight from the late Miocene structural development of the Abert Rim fault, southern Oregon, USA: Tectonophysics, v. 488, p. 71-86.

Sibson, R. H., 1987, Earthquake rupturing as a mineralizing agent in hydrothermal systems: Geology, v. 15, p. 701-704.

Shevenell, L., 1990, chemical and isotopic investigation of the new hydrothermal system at Mount St. Helens, Washington [Ph.D. dissertation]: Reno Nevada, University of Nevada-Reno, 282 pp.

Streck, M. J., and A. L. Grunder, 1995, Crystallization and welding variations in a widespread ignimbrite sheet; the Rattlesnake Tuff, eastern Oregon, USA: Bulletin of Volcanology, v. 57, p. 151-169.

Western Regional Climate Center, Desert Research Institute, 2014, Period of Record Monthly Climate Summary for Fields, Oregon, station ID 352876 (5/1/73 to 3/31/2013), accessed 5/5/2015, http://www.wrcc.dri.edu/cgi-bin/cliMAIN.pl?or2876.